Prediction of Regiospecific Hydroxylation of Camphor Analogs by Cytochrome $P450_{cam}$

Dan Harris* and Gilda Loew

Contribution from the Molecular Research Institute, 845 Page Mill Road, Palo Alto, California 94304

Received November 15, 1993. Revised Manuscript Received September 2, 1994[⊗]

Abstract: The regiospecificities of the hydroxylations of *d*-camphor, *d*-camphane, *d*-thiocamphor, and *d*- and *l*-norcamphor have been predicted by employing geometric criteria obtained from molecular dynamic simulations of enzyme-substrate interactions in conjunction with the thermodynamic criteria of relative radical energetics derived from *ab initio* and semiempirical quantum mechanics. Molecular dynamic simulations were performed using the Amber 4.0 suite of programs with modified Lennard-Jones 6-12 parameters and explicit inclusion of all atoms within a 16 Å "belly" region surrounding the reactive ferryl oxygen center. The predictions were in good agreement with experiment for the three substrates for which hydroxylation data are available for resolved enantiomers. Specifically, camphor hydroxylation is predicted to be completely regiospecific (100% at C_5). Camphane, which cannot hydrogen bond to the enzyme, is found to be hydroxylated 90% at C_5, 9% at C_6, and 1% at C_3. Thiocamphor hydroxylation is predicted to be less regiospecific (85% at C_5 and 15% at C_6) than camphor starting from an orientation similar to that of camphor in the $P450_{cam}$ binding site. The predicted regioselectivities for all three analogs are in excellent agreement with experimental results. Regiospecificities obtained for *d*- and *l*-norcamphor are predictions that remain to be verified. They are not directly comparable with experimental results because hydroxylation products have been determined only for the racemic substrate. The reliability of the constrained protein ("belly") model used was tested for camphor and camphane by performing full protein simulations as well as constrained simulations for these two substrates. The results of both simulations led to comparable predictions of regiospecificity of substrate hydroxylation. These results illustrate the utility of an approximate model of cytochrome $P450_{cam}$ that confines unconstrained dynamic motion to a region around the binding site in making accurate predictions of regiospecificity and stereoselectivity of $P450_{cam}$ hydroxylation for substrates of moderate size.

Introduction

The ubiquitous cytochrome P450 family of isozymes transform largely nonpolar substrates by hydroxylation, epoxidation, and N and S atom oxidation. The architecture of the active site of a given isozyme often accommodates a variety of substrates, but with quite large variations in substrate efficacy and regio- and stereoselective product distributions. The identification and characterization of the steric and electronic determinants of the enzymatic efficiency and regio- and stereoselectivities of products are essential to better understanding of enzyme function. While microsomal P450's have the beneficial effect of elimination of xenobiotics, many of the products of its metabolism are themselves toxic and/or carcinogenic. Thus, understanding the modulation of product distribution can also be very useful in computer-aided risk assessment.

A great deal of evidence, accumulated over many years,[1-3] suggests that cytochrome P450's hydroxylate substrates via an enzymatic cycle that involves (i) entry of the substrate with displacement of most or all of the substrate cavity water; (ii) a change of the ferric heme spin state upon substrate binding that facilitates a change in the redox potential toward one-electron reduction via a complex electron transport system; (iii) a one-electron reduction to a ferrous heme followed by (iv) entry and binding of molecular oxygen to the ferrous heme; (v) a second one-electron reduction; (vi) formation of the reactive intermediate with significant oxygen radical character; and (vii) abstraction of a substrate hydrogen by the radical oxygen intermediate followed by radical recombination to form hydroxylated products. The precise nature of the reactive intermediate has not been definitively determined but is widely believed to be a compound I-type cation-radical ferryl oxygen species, by analogy with the known catalytic intermediate in peroxidase.[4] There is indirect evidence for such a species, e.g. the known incorporation of the single oxygen atom of the dioxygen molecule bound directly to the iron into the substrate. There is also evidence from the kinetic isotope effect that a radical mechanism of hydroxylation involving H abstraction as the rate-determining step is a reasonable one.[5,6]

A number of experimental studies of the regio- and stereospecific metabolisms of a variety of substrates including camphor analogs,[7] styrene analogs,[8] valproic acid,[9] and thioanisoles[10] have now been reported using $P450_{cam}$. Parallel theoretical

[⊗] Abstract published in *Advance ACS Abstracts*, February 15, 1995.

(1) Gungerich, F. P. *Crit. Rev. Biochem. Mol. Biol.* **1990**, *25*, 97-153.

(2) Ortiz de Montellano, P. R. Oxygen Activation and Transfer. In *Cytochrome P-450: Structure, Mechanism, and Biochemistry*; Ortiz de Montellano, P. R., Ed.; Plenum Press: New York, 1986; Chapter 7, pp 217-271.

(3) Pudzianowski, A. T.; Loew, G. H. *Int. J. Quantum Chem.* **1983**, *23*, 1257-1268.

(4) Penner-Hahn, J. E.; Eble, K. S.; Murray, T. J.; Renner, M.; Balch, A. L.; Groves, J. T.; Dawson, J. H.; Hodgson, K. O. *J. Am. Chem. Soc.* **1986**, *108*, 7819.

(5) Atkins, W. M.; Sligar, S. G. *Biochemistry* **1988**, *27*, 1610-1616.

(6) Jones, J. P.; Rettie, A. E.; Trager, W. F. *J. Med. Chem.* **1990**, *33*, 1242-1246.

(7) (a) White, R. E.; McCarthy, M.-B.; Egeberg, K. D.; Sligar, S. G. *Arch. Biochem. Biophys.* **1984**, *228*, 493. (b) Atkins, W. M.; Sligar, S. G. *J. Biol. Chem.* **1988**, *263*, 11842. (c) Atkins, W. M.; Sligar, S. G. *J. Am. Chem. Soc.* **1989**, *111*, 2715.

(8) Ortiz de Montellano, P. R.; Fuetel, J.; Collins, J.; Camper, D.; Loew, G. *J. Am. Chem. Soc.* **1991**, *113*, 3195-3196.

(9) Rettie, A. E.; Baillie, T. A.; Sheffels, P. R.; Chang, Y. T.; Loew, G. H.; Ortiz de Montellano, P. R. In preparation.

(10) Ortiz de Montellano, P. R. Private communication.

0002-7863/95/1517-2738$09.00/0

efforts have been undertaken in our laboratory to predict and understand the origin of the observed product distribution for these diverse types of substrates by $P450_{cam}$.[11,12] In these studies, the relative stabilities of the radicals formed by H atom abstraction at competing C atom positions of the substrate were used as a thermodynamic criteria for preferred hydroxylation sites. This criterion implies that the first step, H abstraction by the ferryl oxygen, is rate determining in hydroxylation and that the rate of reaction is proportional to the stability of the radical intermediate formed in this step. While this property can be calculated for the substrate alone, determination of the appropriate steric criteria requires a knowledge of the 3D structure of the isozyme, since it involves explicit characterization of enzyme−substrate complexes. The study of $P450_{cam}$ provides this opportunity since it is one of three isozymes for which an X-ray structures[13a,b,c] have thus far been reported. The two steric criteria chosen for modulation of regioselectivity hydroxylation were also based on an *H*-abstraction mechanism. They are the distance, H_n-O, between the substrate H atom to be abstracted and the ferryl oxygen atom as well as the angle, $-C_n-H_n-O$, between the C atom to which the H is attached, the H atom, and the ferryl oxygen. These mechanism-based geometric parameters have proven to be fruitful in past studies.[11,12]

In the work reported here, we have employed the same thermodynamic and steric criteria for regioselective hydroxylation, as in past studies described above, to predict and understand the origin of the regioselective hydroxylations of *d*-camphor, *d*-camphane, *d*-thiocamphor, and *d*- and *l*-norcamphor by the putative catalytically active ferryl form of $P450_{cam}$.

The work reported here is an extension of our previously reported studies of four analogs, camphor, norcamphor, pericyclocamphanone, and 5,5-difluorocamphor, in three important ways: (i) We have included the entire protein, in its active ferryl form, in the enzyme−substrate complex characterized and have performed constrained as well as, in two cases for comparison, unconstrained MD simulations. (ii) We have used the dynamic behaviors of the energy-optimized substrate−$P450_{cam}$−I complexes to calculate the distances and angles chosen as the steric criteria for preferred hydroxylation sites. (iii) We have included two new camphor analogs, thiocamphor and camphane, with diminished or no ability to respectively form a H-bond with the Tyr-96 to assess the effect of increased hydrophobic interactions in these substrates on their regioselective hydroxylations. Several full protein simulations of the camphor,[14] norcamphor,[15,16] and thiocamphor[15,16] complexes with $P450_{cam}$ have been reported, but some of these studies do not include the ferryl form required for prediction of regioselective hydroxylation.[14b,16]

In these studies we have employed the high-resolution crystal structures of the ferric states of cytochrome $P450_{cam}$ complexes with these four substrates: camphor,[13] camphane,[18] thiocamphor,[18] and norcamphor.[19] A recent review summarizes the current status of know crystal structures.[20]

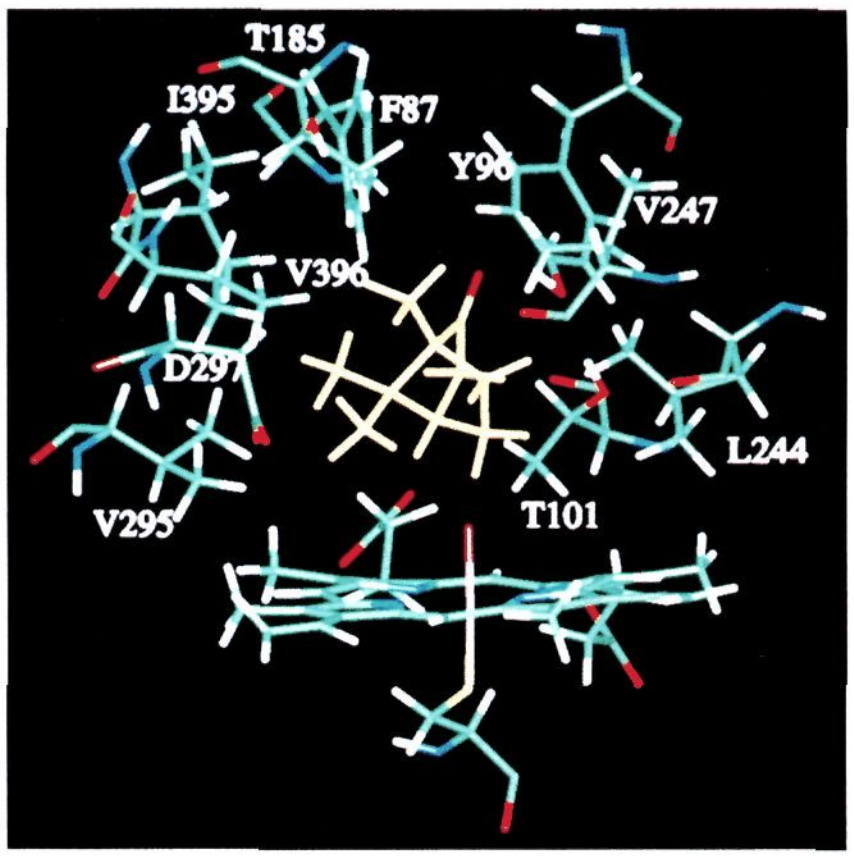

Figure 1. Camphor bound in the $P450_{cam}$ substrate binding site formed by the ferryl form of the heme and numerous hydrophobic residues.

Figure 1 shows that the nonbonded interactions of camphor-like substrates with the binding site of cytochrome $P450_{cam}$ are primarily hydrophobic. Specifically these include contacts with the hydrophobic residues F87, L244, V247, G248, V295, I395, and V396. While a few polar residues, Y96, T101, T185, and D297, also make contact with substrates of $P450_{cam}$, it is only Y96 which appears to interact with substrates through hydrogen bonding. While such a hydrogen-bonding interaction restricts the mobility of substrates about an axis, clearly van der Waals contacts are the primary determinants of camphor-like substrate dynamics since, for example, camphane, a substrate lacking a hydrogen bond accepting group, has a hydroxylation profile very similar to that of camphor.

Table 1 summarizes additional information from both the crystal structures and metabolic studies of the four substrates chosen. All the variants have a camphor-like molecular framework but differ in their molecular volume and ability to hydrogen bond to the enzyme. Camphor, camphane, and thiocamphor have similar molecular volumes but differ in their ability to hydrogen bond to the substrate. The carbonyl group of camphor forms a good hydrogen bond with the OH group of tyrosine-96 in the substrate-bound crystal structure, that camphane cannot form because it lacks the keto group. Consequently, the isotropic *B* factor of camphane in the P450 binding cavity is nearly twice as large as that of camphor (Table 1). However, *d*-norcamphor, which like camphor has a hydrogen bond to the enzyme, nevertheless has a mobility similar to that of camphane, presumably because of its smaller molecular volume and diminished van der Waals contacts, pointing to multiple factors that can modulate substrate mobility. A water is found in the ferric $P450_{cam}$−thiocamphor structure that appears to impede the thioketo moiety from forming a H-bond with the Y96. Instead, thiocamphor is found in two resolvable

(11) (a) Collins, J. R.; Camper, D. L.; Loew, G. H. *J. Am. Chem. Soc.* **1991**, *113*, 2736−2743. (b) Chang, Y.-T.; Loew, G. H.; Rettie, A. E.; Baillie, T. A.; Sheffels, P. R.; Ortiz de Montellano, P. R. *J. Quantum Biol. Symp.*, in press.

(12) Fruetel, P. R.; Collins, J. R.; Camper, D.; Loew, G.; Ortiz de Montellano, P. R. *J. Am. Chem. Soc.* **1992**, *114*, 6987−6993.

(13) (a) Poulos, T. L.; Finzel, B. C.; Howard, H. J. *J. Mol. Biol.* **1987**, *195*, 687−700. (b) Ravichandran, K. G.; Boddupalli, S. S.; Hasemann, C. A.; Peterson, J. A.; Deisenhofer, J. *Science* **1993**, *261*, 731. (c) Boddupalli, S. S.; Hasemann, C. A.; Ravichandran, K. G.; Lu, J.-Y.; Goldsmith, E. J.; Deisenhofer, J.; Peterson, J. A. *Proc. Natl. Acad. Sci. U.S.A.* **1992**, *89*, 5567.

(14) (a) Paulsen, M. D.; Bass, M. B.; Ornstein, R. L. *J. Biomol. Struct. Des.* **1991**, *9*, 187−203. (b) Paulsen, M. D.; Bass, M. B.; Ornstein, R. L. *J. Biomol. Struct. Dyn.* **1991**, *9*, 187−203.

(15) Paulsen, M. D.; Ornstein, R. L. *J. Comput.-Aided Mol. Des.* **1992**, 449−460.

(16) Bass, M. B.; Ornstein, R. L. *J. Comput. Chem.* **1993**, *14*, 541−548.

(17) Paulsen, M. D.; Ornstein, R. L. *Protein Eng.* **1993**, *6*, 359−365.

(18) Raag, R.; Poulos, T. *J. Am. Chem. Soc.* **1991**, *30*, 2674−2684.

(19) Raag, R.; Poulos, T. *Biochemistry* **1989**, *28*, 917−922.

(20) Raag, R.; Poulos, T. *Front. Biotransform.* **1991**, *7*, 1.

Table 1. Summary of Parameters Descriptive of Enzyme Substrate Interactions, Regiospecificity of Hydroxylation, and Hydroxylation Efficiency of $P450_{cam}$[a]

substrate	mol volume of substrate (Å^3)	H-bond to Y96	avg substrate *B* factor (Å^2)	ligand water	regiospecificity of hydroxylation	hydroxylation efficiency
camphor	315	yes	16.2	no	5-exo (100%)[b,c,d]	100%[c]
camphane	309	no	30.1	yes	5-exo (90%)[c] 6-exo (10%)	5%[c]
norcamphor	236	yes	33.5	yes	5-exo (45%)[d] 6-exo (47%) 3-exo (8%)	12%[d]
thiocamphor	322	no	23.5	yes	5-exo (64%)[c] 6-exo (34%) 3-exo (2%)	98%[c]

[a] Crystallographic information from this table extracted from ref 13. [b] Reference 5a. [c] Reference 5b. [d] Reference 5c; regiospecificity determined for *d,l*-norcamphor racemate.

orientations in the substrate-bound ferric form, both with the thioketo group near the heme iron.

The results of the molecular dynamics simulations described here were used to obtain the Hn−O distances and Cn−Hn−O angles used as steric criteria for prediction of hydroxylation product distribution. In addition, assuming that H atom abstraction is the rate-determining step, the relative stabilities of the radicals formed at each C position in these four substrates were used, as in our previous work, as the electronic modulators of hydroxylation product distribution. Finally, the protein model and parameter refining needed to obtain reliable steric criteria using the Amber 4.0 suite of programs were examined. The success of the studies here provide a guideline for protocols than can be reliably used to examine other families of substrates.

Computational Procedures/Methodology

Crystallographic coordinates of the *d*-camphor, *d*-camphane, and *d*-norcamphor complexes with the ferric state of $P450_{cam}$, including crystallographic waters, were used for the initial structure of all but the ferryl oxygen and H atoms in the ferryl−protein substrate complex. In the case of thiocamphor, the substrate was docked in an initial orientation like camphor with the S atom replacing the O atom as the H-bond acceptor in H bonding to the Tyr-96 OH group. *l*-Norcamphor was docked in a configuration like that of *d*-norcamphor with respect to its ring atom positions. In this study, we have assumed that the waters in the crystal structures of camphane, norcamphor, and thiocamphor that appear as the sixth ligand of the iron in the substrate-bound ferric heme are displaced by the ferryl oxygen in compound I formation and have removed it in simulations of the ferryl complexes with camphane, norcamphor, and thiocamphor.

Molecular dynamics trajectories (150 ps) of the substrate-bound forms of camphor, camphane, thiocamphor, and norcamphor were performed to assess "reactive" energetically accessible geometries of the enzyme−substrate complexes with the P450 heme in compound I form. If compound I is long lived with respect to the time scale of substrate reorientation in the enzyme−substrate cavity, the molecular dynamics trajectories may be thought of as probing actual time-dependent enzyme−substrate complexes prior to "reaction". In the case that the compound I form in P450 is sufficiently reactive/short lived that the initial configuration of the enzyme−substrate complex after compound I formation is the reactive configuration, the fraction of thermodynamically assessable configurations sampled in an MD trajectory will nevertheless provide reliable estimates of the most probable initial configurations of the enzyme−substrate configuration.

Molecular dynamics simulations were conducted using AMBER 4.0.[21] However, simulations of camphor in the binding pocket of $P450_{cam}$ with use of standard AMBER van der Waals parameters were found to exhibit excessive rotational dynamics in contradiction to X-ray structural studies and led to predictions of 79% at C_5 and 21% at C_6 hydroxylation for camphor in contradiction to the complete regiospecificity of hydroxylation observed at the C_5 position (100% at C_5). Therefore, it appears that van der Waals interactions are somewhat underestimated for this type of substrate. To test the hypothesis that particularly C−C and C−H van der Waals parameters are not sufficiently large to predict the relative enzyme−substrate dynamics of the substrates of interest in this study, we have used alternative Lennard-Jones[6−12] parameters for all sp^3 and sp^2 carbons and hydrogens imported from the BIOSYM CVFF[22] force field summarized in Table 2. As shown in this table, the van der Waals radii (R^*) of aromatic and aliphatic carbons and hydrogen in the AMBER 4.0 are smaller than those from CVFF-BIOSYM force fields. We have made this revision in the force field to determine if somewhat enhanced van der Waals interaction can consistently explain the regioselectivities of the hydroxylations of all four substrates.

Table 2. Modified van der Waals Parameters Imported into AMBER 4.0

	amber		CVFF	
amber atom type	$R^*/2$[a]	ϵ[b]	$R^*/2$	ϵ
sp^3 carbons[c]	1.80	0.06	1.95	0.16
sp^2 carbons[d]	1.85	0.120	2.03	0.148
hydrogens[e]	1.54	0.01	1.375	0.03

[a] $R^*/2$ is one-half the minimum energy separation for two atoms. [b] ϵ is the well depth for two atoms. [c] Type CT in AMBER. [d] Type C in AMBER. [e] Type HC in AMBER.

Computed atomic isotropic *B* factors, while showing similar trends with residue number, are smaller for the modified set; the mean protein atomic *B* factor is 23 Å^2 for the AMBER set and 15 Å^2 for the modified set for simulations of camphor-bound $P450_{cam}$ compared to the experimental value of 18 Å^2. The mean atomic *B* factor for the substrate however is 20 Å^2 for the modified set and 60 Å^2 for the AMBER set compared to the X-ray value of 16 Å^2 in the camphor-bound crystal structure. Clearly, the usage of the modified set results in a compromise in the quality of the predictions in the protein atom and substrate fluctuations. A check of other structural features such as rms deviations from crystal structures and stabilities of hydrogen bond networks using the modified van der Waals set reveals no significant distortions. Additionally, precedent exists for such alteration by the developer of ABMER itself.[21] The importation of the CVFF-BIOSYM parameters is thus a means of exploring the impact of modest modification of the van der Waals parameterization upon the particular types of predictions made in this work, predictions sensitive to the rotational dynamics of pseudospherical substrates of $P450_{cam}$.

The Fe-O bond distance was taken to be 1.70 Å as found in XAFS studies[23] and a force constant of 200 kcal/Å used. Atomic charge representations for substrates were obtained as electrostatic potential derived charges from AM1 calculations by employing the method of Singh and Kollman which employs three shells and point density of 5 points/Å on each surface.[24] Net atomic charges for the cysteinate−heme compound I complex were derived from a ZINDO calculation

(21) Pearlman, D. A.; Case, D. A.; Caldwell, J. C.; Seibel, G. L.; Singh, U. C.; Weiner, P.; Kollman, P. A. *AMBER UCSF Version 4.0*; Department of Pharmaceutical Chemistry, University of California: San Francisco, CA, 1991, 1986).

(22) Biosym Corp., San Diego, CA.

(23) Dawson, J. H.; Kau, L.-S.; Penner-Hahn, J. E.; Sono, M.; Eble, K. S.; Bruce, G. S.; Lowell, P. H.; Hodgson, K. O. *J. Am. Chem. Soc.* **1986**, *108*, 8114−8116.

(24) Singh, U. C.; Kollman, P. A. *J. Comput. Chem.* **1984**, *5*, 129−145.

for the a_{2u} radical cation, corresponding to a quartet electronic configuration of $d_{x^2-y^2}^2\, a_{2u}^1\, d_{xz}^1\, d_{yz}^1$ [25,26] found to be the ground electronic state. The use of such ZINDO charges should provide a reasonable semiquantitative estimate of the electrostatic interactions with the heme compound I form since the electronic structure results from this method lead to calculated electronic and spectroscopic properties in good agreement with experiment. The values of the charges in our model are included in the form of the AMBER prep file and are available as supplementary material.

Each of the substrate-bound P450 complexes was energy minimized using AMBER 4.0 by using 100 steps of steepest descents followed by 1900 steps of conjugate gradients. The gradient at this point was typically 0.8 kcal/Å. The positions of the hydrogen atoms attached to oxygen and nitrogen were then modified by short dynamics runs of 5−10 ps at 350 K. The structure was equilibrated for 15 ps at 300 K by loosely coupling the system to a heat bath and employing a series of gradually decreasing harmonic coordinate constraints. The system was then further equilibrated for about 25 ps before accumulation of dynamics data for analysis. Following he equilibration procedure, molecular dynamics runs were continued for 150 ps. In most of the simulations, a constrained "belly" option was used that allowed explicit motions of all atoms within a 16 Å region surrounding the ferryl oxygen. All residues inside the unconstrained region were treated in the all-hydrogen representation. Residues in the constrained regions were treated in the polar-H (united atom) representation. For comparison, full protein simulations were performed for camphor and camphane-bound $P450_{cam}$ by employing the all-hydrogen representation for the entire protein. Nonbonded interactions were truncated at a relatively long distance of 15.0 Å in order to minimize the large forces associated with truncations in the nonbonded interactions. In order to compensate for the absence of water solvating the protein, we have employed a radially dependent dielectric constant of $D = r$, where r is the interatomic distance for the atom pair electrostatic contribution being computed. The use of this relatively long nonbonded cutoff and a radially screened dielectric constant resulted in retention of all crystallographic waters in the simulation and minimal contraction of the protein. The radius of gyration of the protein was found to be ca. 21.1 Å following minimization and equilibration and did not change significantly during the full protein camphor or camphane simulations. This radius of gyration was similar to that found in short simulations of the protein with a 5 Å solvent shell (21.4 Å), employing a dielectric constant of unity. The use of a radial dielectric is essential for conservation of energy in conjunction with the Berendsen coupling algorithm[27] in simulations not including water of solvation.[28]

A total of 600 structures saved at 0.25 ps intervals during the 150 ps of equilibrated dynamics trajectories were used to calculate the ferryl oxygen−substrate hydrogen distance and the ferryl oxygen−substrate hydrogen−substrate carbon bond angles which were used as steric determinants of the hydroxylation product distribution.

The energies of radicals formed by H abstraction at all positions in the substrates were calculated using AM1[29] and unrestricted Hartree−Fock procedures for a doublet state. Radicals were fully energy optimized using this procedure and the vibrational frequencies of the optimized structures evaluated to assure convergence to a minimum rather than a saddle point.

As a check on the rasonableness of the relative energies obtained from these UHF AM1 calculations, the radical energies for the 5-, 6-, and 9-position camphor radicals were calculated using *ab initio* calculations including MP2 post-Hartree−Fock corrections. Since results for radical energetics calculated using 3-21G and 6-31G* basis sets are similar,[30] typically differing from experimental values by 1−2 kcal/mol, the 3-21G basis set was used for geometry optimization followed by a single pint 3-21G** MP2 calculation at this geometry to examine the effects of correlation on the energy differences. The

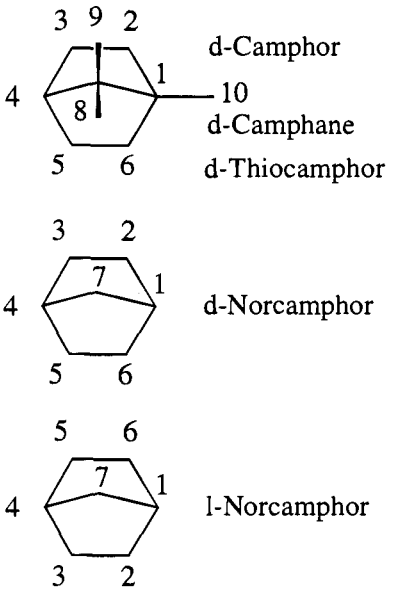

Figure 2. Carbon framework numbering for the camphor analog in this study.

Table 3. Comparison of Relative Radical Energetics[a] Computed using *Ab Initio* and Semiempirical Methods

parent molecule	position radical type[b]	ΔE_{AM1}	$\Delta E_{3\text{-}21G}$	$\Delta E_{3\text{-}21G^{**}/MP2}$[c]	expt
camphor	C5 (2°)	0.0	0.0	0.0	
	C6 (2°)	+0.24	−0.60	−0.46	
	C9 (1°)	+1.61	+0.91	+0.87	
propane	C2 (2°)	0.0	0.0	0.0	0.0
	C1 (1°)	+5.69	+2.40	+1.81	+2.8
isobutane	C2 (3°)	0.0	0.0	0.0	
	C1 (1°)	+10.39	+3.79	+2.65	

[a] Relative energies in units of kcal/mol. [b] 2° implies a secondary radical center, and 1° implies a primary radical center. [c] An 3-21G**/MP2/3-21G calculation.

ab initio calculations were performed using Gaussian 92.[31] In all cases, excess spin density was verified to be primarily on the C center of the radical from which the H was abstracted. No spin contamination was obtained for any radical.

Results and Discussion

In order to assess whether there are significant energy differences between primary and secondary radicals of camphor-like substrates and whether semiempirical methods may be employed rather than *ab initio* calculations to evaluate radical energetics, we have calculated the relative energetics of the 5-, 6-, and 9-position radicals of camphor and of the primary and secondary C atom of propane and isobutane using *ab initio* and semiempirical AM1 calculations. Figure 2 shows the numbering of the carbon centers of the substrates involved in this work. The results of these calculations of relative radical energies are shown in Table 3. The results for the isopropyl radical compared to experiment indicate that, while AM1 calculations are able to predict the correct ordering of radical stabilities, they overestimate the radical energy differences for this simple aliphatic system. The results also suggest that an *ab initio* calculation with a modest basis set is in better agreement with

(25) Du, P.; Loew, G. H. *Int. J. Quantum Chem.* **1992**, *44*, 251−261.
(26) Harris, D. Unpublished calculations.
(27) Berendsen, H. J. C.; Postma, J. P. M.; van Gunsteren, W. F.; DiNola, A.; Haak, J. R. *J. Chem. Phys.* **1984**, *81*, 3684.
(28) Guenot, J.; Kollman, P. A. *J. Comput. Chem.* **1993**, *14*, 295−311.
(29) Stewart, J. J. MOPAC 6.0, OCPE Program 455, Bloomington, IN.
(30) Ibrahim, M. R.; Schleyer, P. v. R. *J. Comput. Chem.* **1985**, *6*, 157−167.
(31) Gaussian 92, Revision C; M. J. Frisch, G. W. Trucks, M. Head-Gordon, P. M. W. Gill, M. W. Wong, J. B. Foresman, B. G. Johnson, H. B. Schlegel, M. A. Robb, E. S. Replogle, R. Gomperts, J. L. Andres, K. Raghavachari, J. S. Binkley, C. Gonzalez, R. L. Martin, D. J. Fox, D. J. Defrees, J. Baker, J. J. P. Stewart, and J. A. Pople; Gaussian, Inc.: Pittsburgh PA, 1992.

Table 4. Table of Relative Energies[a] of Radicals from UHF AM1 Calculations

position	camphor	camphane	norcamphor	thiocamphor
C2		0.11		
C3	1.61	0.00	1.76	*b*
C4	16.61	15.88	16.22	16.80
C5	0	0	0.00	0.00
C6	0.24	0.23	0	0.18
C7			4.36	
C8	1.75	1.32		1.55
C9	1.53	1.55		1.53
C10	2.12	2.21		2.60

[a] Energies relative to the most stable radical in units of kcal/mol. [b] The value of $\langle S^2 \rangle$ for this radical was 0.9, indicating spin contamination.

experiment. For camphor, the AM1 and *ab initio* calculations are in qualitative agreement in that they both suggest only modest energy differences between different secondary C atom positions, C_5 and C_6, and slightly larger differences between the secondary and primary C radicals studied. The single point ab initio results suggest that inclusion of polarization functions and post-Hartree–Fock corrections did not alter the ordering of camphor radical stability. It thus seems unlikely that optimization with a much larger basis set would dramatically alter the general character of these results. Thus, one may conclude that AM1 calculated energy differences between primary and secondary and primary and tertiary radicals can be used as qualitative indicators of relative radical stabilities.

Table 4 gives the relative radical energies obtained for all C-atom sites, relative to the most stable radical in each of the four camphor analogs studied. In general, the same pattern is observed for each substrate. Bridgehead C4 radicals are extremely unstable, and sufficient energy differences are obtained for formation of primary and secondary radicals to provide a thermodynamic/electronic criteria for discrimination.

A consideration of the relative radical stabilities of camphor-like substrates shows most secondary radical sites to be of nearly equal energies while the primary radical sites are approximately 1.5 kcal/mol^{-1} less stable than secondary sites. Given comparable geometric probabilities for reaction of a primary and secondary hydrogen, one would expect the relative probability of radical formation to be roughly proportional to a Boltzmann distribution in the relative radical energetics: $\exp(-(E(2°) - E(1°)/kT)$. Simultaneous exposure of secondary and primary sites are therefore expected to give ca. 97% formation of a secondary radical site. We therefore employ the criteria that, given simultaneous exposure of secondary and primary centers, the radical produced via abstraction by the ferryl oxygen will be exclusively secondary radicals. This is the "electronic"/thermodynamic criteria employed to predict relative regiospecificity of hydroxylation of camphor analogs.

Table 5a,b summarizes the results of analysis of the trajectories of camphor in the binding site of $P450_{cam}$ using the structures stored during MD simulation leading to the prediction of the hydroxylation regiospecificity of *d*-camphor. Shown in these tables are the results from both constrained and full protein molecular dynamic simulations as well as two different geometric criteria used to define an active substrate–enzyme complex geometry with differing minimum CH- - -O=Fe distances. In these tables, under the column headed "steric" are the percentages of the stored structures in which the H atom on the specified carbon center was found to be close enough to be abstrated by the ferryl oxygen atom using the two cut-off values of 2.7 Å (Table 5a) and of 3.4 Å (Table 5b) chosen, each with a O- - -H_n–C_n angle deviating from linearity by ±45°.

Table 5. Prediction of Hydroxylation Regiospecificity of *d*-Camphor using Different Computational Models

	belly		full protein	
atom	steric[a]	steric + elect.	steric	steric + elect.
	(a) $R_{REACT} = 2.7$ Å ± 45°			
C3				
C4	0.3%			
C5	87.0%	100.0% (exo)	85.0%	99.9% (exo)
C6			0.1%	0.1% (exo)
C8	12.7%		14.9%	
C9				
C10				
fraction hits[b]	407/600		574/600	
	(b) $R_{REACT} = 3.4$ Å ± 45°			
C3				
C4	0.3%			
C5	64.9%	97.2% (exo)	66.6%	99.8% (exo)
C6	1.85%	2.7% (exo)	0.1%	0.2% (exo)
C8	32.9%		33.3%	
C9				
C10				
fraction hits[b]	424/600		582/600	

[a] The numbers in this column are the number of MD configurations out of the total number, expressed as number of reactive configurations/total number of configurations, with an H_n–O distance and C_n–H_n–O angle within the specified range. [b] These are the fraction of MD configurations which were "reactive" configurations, anticipated to lead to hydroxylated product.

With the percent hydroxylation predicted at each site, using steric criteria alone, this value can be obtained directly from the values given in the "steric" column of the molecular dynamics simulation of the camphor–enzyme complex. These results indicate hydroxylation would occur primarily at the C_5 position but with a significant amount of C_8–OH formed. These results are very similar for both the constrained and full protein simulations. When the minimum distance at which H abstraction is presumed to occur is increased to 3.4 Å (Table 5b), the percentage of primary hydroxylation product predicted is even greater in both the constrained and full protein MD simulations. Including the thermodynamic criteria, based on the preference for secondary radical over primary radical formation, eliminates the primary C-hydroxylation sites and leads to prediction of complete regioselective hydroxylation at C_5, in excellent agreement with experiment for both constrained and full MD models and with different cut-off values for the distance of approach of the hydrogen atom to the ferryl oxygen cutoff chosen. The only difference between the two cut-off values used, as shown in Table 5a,b, is that the longer one led to a somewhat higher fraction of "snapshots" within the reactive range to be included, the statistics determining the regioselectivity. However, for both distances chosen, there is a very high percentage of structures in which some H atom is close enough to react with the ferryl oxygen.

The stereochemistries of the 5-hydrogen abstraction as determined from reactive geometries of camphor in the active site for the trajectories are also summarized in Table 5 and are both 5-exo abstraction. Experimental studies of isotopically labeled camphor suggests that abstraction of both 5-exo and 5-endo hydrogens leads primarily to 5-exo product.[32] Thus, apparently for camphor, formation of the 5-exo product is favored irrespecive of which hydrogen is initially extracted. The results for final product distribution are then in accord with experiment assuming 5-exo hydrogen abstraction proceeds to the 5-exo hydroxy product without inversion of configuration. These results are also in excellent accord with previously

(32) Gelb, M. H.; Heimbrook, D. C.; Malkonen, P.; Sligar, S. G. *Biochemistry* **1982**, *21*, 370.

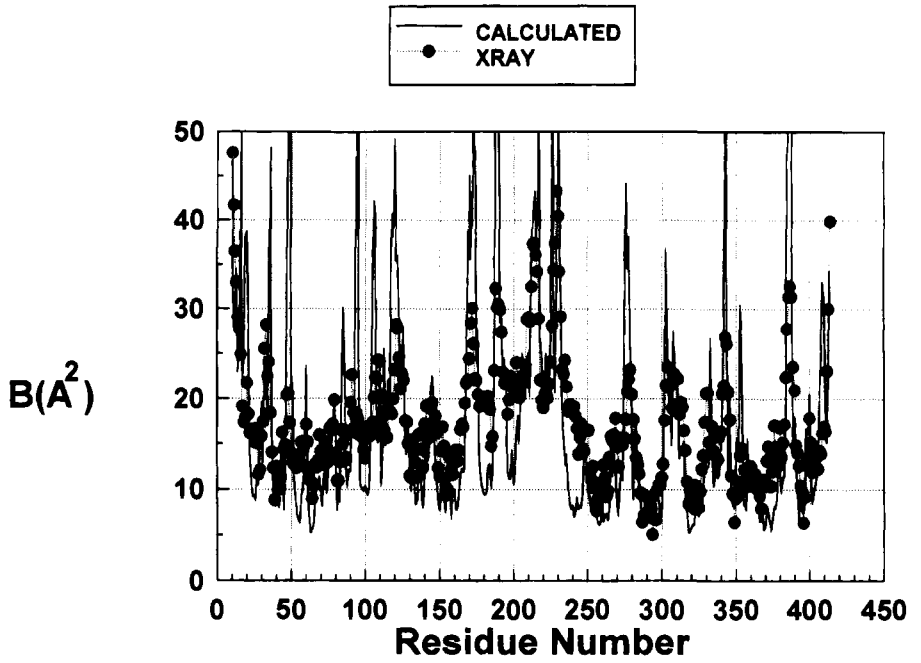

Figure 3. Comparison of Ca atom *B* factors from a full protein simulation of camphor-bound P450$_{cam}$ with those obtained from crystallographic studies.

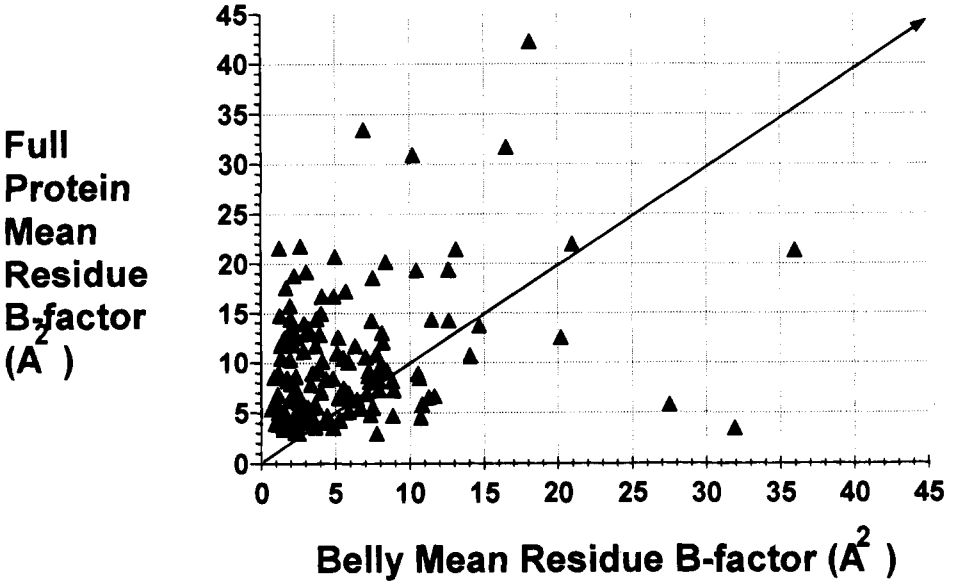

Figure 4. Comparison of mean residue *B* factors from full protein and constrained molecular dynamics of the camphor-bound P450$_{cam}$ complex.

reported theoretical results in which a hydroxylation efficiency of 100% at C_5 was found for camphor.[15]

The two main insights gained from these studies for camphor are (i) only if steric and electronic criteria are included is there excellent agreement obtained with experiment and (ii) both constrained (belly) and unconstrained full protein dynamics give equally good results that are insensitive to the cut-off value used to assess the reactive H atoms.

Although both constrained and unconstrained MD simulations lead to similar results for camphor, there is some reason to be concerned about differences in the C atom isotropic *B* factors derived from each of these simulations. Figure 3 shows comparisons of the *B* factors derived from the X-ray crystallography with those derived from the full protein simulation used to calculate the hydroxylation results for camphor, while Figure 4 compares the *B* factors obtained from the unconstrained and constrained MD smulations. Figure 3 indicates general qualitative agreement of the full MD simulations with the observed values. Figure 4 shows that, due to the constraints imposed on residues outside the 16 Å region, the fluctuations of these amino acids within the unconstrained region are biased and systematically distorted compared to results from unconstrained MD simulations.

While the results for pseudospherical camphor-like substrates do not appear to be substantially affected by such constraints, it is not clear that such constraints will not distort the dynamics of other qualitatively different substrates. Thus, in order to further investigate the validity of using constrained MD simulations for prediction of regioselective hydroxylation of camphor-like compounds, we chose a second substrate camphane to compare full and constrained protein MD simulations. The architecture and size of camphane (residue volume = 309 Å^3) are very similar to those of camphor (molecular volume = 315 Å^3). It differs, however, in the important respect that it lacks the keto group by which camphor hydrogen bonds to tyrosine-96 of P450$_{cam}$.

Table 6. Prediction of Hydroxylation Regiospecificity of *d*-Camphane using Different Computational Models

	belly		full protein	
atom	steric[a]	steric + elect.	steric	steric + elect.
	(a) $R_{REACT} = 2.7$ Å $\pm 45°$			
C2				
C3	1.0%	1.2% (exo)	0.4%	0.8% (endo)
C4	0.2%		4.6%	
C5	75.1%	90.2% (2.1% endo)	52.5%	95.9
C6	7.1%	8.6% (exo)	1.7%	3.3
C8	15.8%		3.6%	
C9			37.1	
C10	0.8%			
fraction hits[b]	443/600		510/600	
	(b) $R_{REACT} = 3.4$ Å $\pm 45°$			
C2				
C3	1.0%	1.2% (exo)	0.4%	0.9%
C4	0.2%		6.0%	
C5	75.1%	90.2% (2.1% endo)	42.8%	93.0%
C6	7.1%	8.6% (exo)	6.1%	6.1%
C8	15.8%			
C9			3.6	
C10	0.8%		44.2	
fraction hits[b]	443/600		510/600	

[a] The numbers in this column are the number of MD configurations out of the total number, expressed as number of reactive configurations/ total number of configurations, with an H_n-O distance and C_n-H_n-O angle within the specified range. [b] These are the fraction of MD configurations which were "reactive" configurations, anticipated to lead to hydroxylated product.

Table 6 shows results for the prediction of the regiospecificity of hydroxylation for *d*-camphane from results of the constrained and full protein MD simulations. We see that, using steric criteria alone, C_5-exo-OH is predicted to predominate, and small amounts of C_6-exo-OH are predicted, consistent with experimental observation. However, the second most abundant product is predicted to be the primary alcohols C_8-OH or C_9-OH, that are not observed. Table 6 also shows that there are significant differences in the percentages of the predicted products using steric criteria alone for the constrained and unconstrained simulations. However, if both steric and electronic criteria are used, excellent agreement with the experimental prediction of C_5/C_6:90%/10% is obtained and the results are comparable for the constrained and full protein dynamics simulations. This reaction profile results from some rotations of this substrate during the 150 ps trajectory to a position with both the C_5 and C_6 camphane carbons proximate to the ferryl oxygen. This table also shows that the predicted products are of exo stereospecificity with only about 2% of the C_5 product predicted to precede by C_5-endo hydrogen abstraction. Experimental results for camphane are reported to be all exo product. All of the predicted C_6 product is predicted to result from C_6-exo hydrogen abstraction.

The similarity of the experimental results for camphane and camphor illustrate that van der Waals contacts alone must be sufficient to determine the high regiospecificity of their hydroxylation given that replacement of the keto group in camphor with two aliphatic hydrogens in camphane only moderately alters the regiospecificity. Particularly the nonbonded contacts of the C_8 and C_9 bridgehead carbons with F87, T185, V295, and V396 and the C_{10} methyl with residue V247 are essential determinants of the rotational dynamics of the camphor-like molecular framework. The comparison between full protein and constrained MD simulations for camphor-like substrates with and without a polar group that can H-bond to the enzyme verifies that both types of simulations lead to comparable predictions of product regioselectivity. Therefore, for the remaining two substrates, only constrained MD simulations were performed.

Table 7. Prediction of Hydroxylation Regiospecificity of *d*-Thiocamphor using Constrained MD Simulations

	$R_{REACT} = 2.7 \pm 45°$		$R_{REACT} = 3.4 \pm 45°$	
atom	steric[a]	steric + elect.	steric	steric + elect.
C2				
C3				
C4				
C5	32.9%	86.2% (exo)	32.2%	85.0% (exo)
C6	5.3%	13.8% (exo)	5.7%	15.0% (exo)
C8	61.8%		62.0%	
C9				
C10				
fraction hits[b]	596/600		598/600	

[a] The numbers in this column are the number of MD configurations out of the total number, expressed as number of reactive configurations/ total number of configurations, with an H_n-O distance and C_n-H_n-O angle within the specified range. [b] These are the fraction of MD configurations which were "reactive" configurations, anticipated to lead to hydroxylated product.

Table 7 shows the results derived from trajectories of *d*-thiocamphor in the binding site of $P450_{cam}$. These results were obtained using a starting structure of this substrate analogous to that of camphor, with the S replacing the carbonyl oxygen in H bonding to the OH group of the Tyr-96. This orientation was chosen in preference to the *d*-thiocamphor orientations found in the ferric crystal structures because, in the ferryl form of the enzyme, it is the preferred orientation due to the repulsive interactions of the sulfur of the substrate and the ferryl oxygen. Using an initial geometry for the ferryl form of the enzyme in which the substrate was in either of its orientations found in the X-ray structure of the ferric state, the thiocamphor was found to immediately rotate to orientations with its thioketo group interacting with the Y96 hydrogen. This latter configuration led to a more stable complex in which the the enzyme−substrate interactions had an interaction energy ca. 20 kcal/mol^{-1} lower than in either of the crystallographic orientations. This enhanced stability is due not only to significant interaction of the oppositely charged Y96 hydrogen and thiocamphor sulfur but also to the elimination of the destabilizing repulsive interaction of the like charged thioketo group of thiocamphor and the ferryl oxygen.

As seen in Table 7, with an initial camphor-like orientation, steric criteria alone strongly favor C_8-OH hydroxylation of thiocamphor. As with the other substrates, but particularly for thiocamphor, only when thermodynamic criteria are also invoked do the predictions from the thiocamphor simulations ca. 85% at C_5 (exo) and 15% at C_6 (exo) give good agreement with the stereospecific experimental results for *d*-thiocamphor of 64% at C_5, 34% at C_6, and 2% at C_3 and with previously results reported from full protein simulations of 70% at C_5, 26% at C_6, and 4% at C_3.[15] The small amount of C_3 product found indicates that thiocamphor in the substrate cavity has most of its reactive configurations with its thioketo group interacting with Y96. However, also the effects of weaker interactions of the thioketo S group with the hydroxy group of Y96 and its increased van der Waals interactions combine to alter the rotational characteristics of this substrate from that of camphor and consequently affect the overall hydroxylation profile.

The evaluation of the norcamphor results is complicated by the fact that experimental results are only known for the enantiomeric mixture. In addition, the fraction of reactive geometries from a norcamphor/$P450_{cam}$ trajectory is approximately one-half that of a trajectory of camphor, camphane, or thiocamphor, suggesting that additional sampling is required to obtain adequate statistics. This reduction in reactive configurations is, in part, caused by the fact that H atoms are further

Table 8. Prediction of Hydroxylation Regiospecificity of *d*- and *l*-Norcamphor from Constrained MD Simulations

(A) Results for Two Trajectories for *d*-Norcamphor

	trajectory 1		trajectory 2[b]	
atom	steric[a]	steric + elect.	steric	steric + elect.
C1				
C3			8.4%	24.5% (18.5% exo)
C4				
C5	92.2%	95.1% (94.0% exo)	5.3%	15.5% (8.8% exo)
C6	4.3%	4.5% (all exo)	20.5%	60.0% (all exo)
C7	3.5%		65.8%	
fraction hits[c]	325.0/600		316.1/600	

(B) Results for Two Trajectories of *l*-Norcamphor

	trajectory 1[d]		trajectory 2	
atom	steric[a]	steric + elect.	steric	steric + elect.
C1				
C3			22.9%	32.9% (all exo)
C4				
C5	29.2%	45.1% (26.4% exo/18.7% endo)	29.0%	41.7% (37.7% exo/4.0% endo)
C6	35.5%	54.9% (52.5% exo/2.4% endo)	17.6%	25.3% (all exo)
C7	35.3%		30.5%	
fraction hits[c]	386.1/600		419.9/600	

(C) Average of *d*- and *l*-Norcamphor Trajectories

atom	average *d*-norcamphor	average *l*-norcamphor
C1		
C3	6.3% (4.7% exo)	17.7% (17.7% exo)
C4		
C5	75.0% (72.5% exo)	43.3% (32.5% exo)
C6	18.7% (18.7% exo)	38.9% (37.8% exo)
C7		

[a] The numbers in this column are the number of MD configurations out of the total number, expressed as numbers of reactive configurations/total number of configurations, with an H_n-O distance and C_n-H_n-O angle within the specified range. [b] The first trajectory for *d*-norcamphor was started from the energy-minimized *d*-norcamphor crystallographic orientation. The second trajectory was started from a minimized docked orientation which resulted in both C5 and C6 positions of *d*-norcamphor being proximate to the ferryl oxygen. [c] These are the fraction of molecular dynamics configurations which were "reactive" configurations, anticipated to lead to hydroxylated product. [d] The initial configurations of the substrate in the *l*-norcamphor−$P450_{cam}$ trajectories were similar in that the C5 position of *l*-norcamphor (cf. Figure 2) was closest to the ferryl oxygen. The two trajectories differed in that the *l*-norcamphor orientation in the first trajectory had initial endo exposure to the ferry oxygen while its orientation in the second had initial exo exposure.

away from the ferryl oxygen in this small substrate, and when it is in a configuration that allows H bonding of its carbonyl group to Y96, it also diminished van der Waals interactions with hydrophobic residues in the cavity. Table 8A,B therefore, presents results from two simulations representing two somewhat different orientations of each enantiomer, in order to obtain statistics equivalent to the other three substrates. The $P450_{cam}$−norcamphor optimized interaction energies of these two different complexes differ by ~2 kcal/mol^{-1}.

Table 8A summarizes the results obtained for *d*-norcamphor. The first trajectory of *d*-norcamphor was started from the energy-minimized crystallographic orientation of *d*-norcamphor in the cavity, while the second trajectory is based on a docked geometry with *d*-norcamphor slightly rotated in the substrate cavity. The results from the two simulations are seen to yield different regiospecificities. The first trajectory resulting in 90% at C_5, while the second leads to a product distribution $C_6 > C_3 > C_5$−OH. The decreased regiospecificity observed in this simulation results in transient Y96−norcamphor hydrogen bond breaking during this trajectory, permitting greater rotation of the substrate in the $P450_{cam}$ substrate cavity. The average results from these two simulations of *d*-norcamphor are shown in Table 8C. The results indicate 75% at C_5 with lesser amounts of C_6-exo (19%) and C_3 (6%) and also indicate that the products are predominantly of exo stereochemistry. These results are in good accord with the work of Paulsen and Ornstein, who studied the hydroxylation of *d*-norcamphor, employing full protein simulations and using a ferryl oxygen-bound heme model, and predicted *d*-norcamphor to be hydroxylated 70% at C5, 26% at C6, and 4% at C3 using the Insight CVFF forcefield.[15]

Table 8B shows the results of two *l*-norcamphor trajectories, both from orientations of the *l*-norcamphor framework like that of *d*-norcamphor in the *d*-norcamphor−$P450_{cam}$ crystal structure. In this orientation, the C_7 bridgehead carbon position of the norcamphor stereoisomers (cf. Figure 2) is near V295, D297, and V396 (see Figure 1). The two docked orientations of *l*-norcamphor optimized the hydrogen bonding of *l*-norcamphor to Y96. Energy minimization of these docked geometries led to the C_5 position of *l*-norcamphor being proximate to the reactive ferryl oxygen. While these two orientations differ only slightly from one another, the first permitted greater exposure of the endo hydrogens of C_5 and C_6. The first trajectory indicates nearly equal amounts of C_5 and C_6 product with a slight excess of C_6. The second trajectory sampled enzyme−substrate geometries resulting in 42% at C_5, 25% at C_6, and 33%/C_3. The C_3 product formed in this trajectory results from the presence of a water in the cavity that forms a hydrogen bond with Y96 after 100 ps of simulation, replacing the Y96 norcamphor hydrogen bond. The results from this trajectory suggest that substrates of smaller of different architecture than camphor may permit disordered solvent in the cavity[20] and that the addition of such water could, in principle, modify the regiospecificities of products formed. The average results for the two *l*-norcamphor trajectories shown in Table 8C indicate 43% at C_5, 39% at C_6 and 18% at C_3. Thus, for both the *l*- and *d*-enantiomers, the C_5 is predicted to be favored, although it is

more dominant for the *d*-enantiomer. The result is in contrast to the previous simulations of the *d*- and *l*-forms starting from multiple orientations of norcamphor but employing the resting state rather than the ferryl state of the enzyme.[16] These workers determined that *d*- and *l*-norcamphor gave opposite preferences for C_5 vs C_6 product.

The results for norcamphor are qualitatively consistent with the experimental results for the four substrates studied; norcamphor is predicted to have the most C_6 relative to C_5 product and the greatest amount of C_3 hydroxylated product. The results for nocamphor also illustrate that the smaller molecular volume and reduced van der Waals contacts lead to the least regiospecific distribution of hydroxylated product of the four substrates studied. In addition to the greater mobility of norcamphor enantiomers leading to a nearly equal distribution of C_5 and C_6, three different dynamical motifs have been observed to give rise to C_3 product. The first involves transient rotations of sufficient amplitude in the cavity to expose C_3 hydrogens. The second is transitory replacement of the Y96- - -norcamphor hydrogen bond by a water proximate to the binding site, and the third is a severing of the Y96- - -camphor hydrogen bond simultaneous with hydrogen bonding of Thr-101 to Y96. Such enzyme−substrate hydrogen bond breaking is absent in the trajectories obtained for camphor and thiocamphor. The greater molecular volume and intimate van der Waals contacts of the methyl substituents of the latter substrates with hydrophobic residues in the $P450_{cam}$ binding site reduce the rotational mobility of these substrates and reduce the likelihood of entry of water into the substrate cavity. Both of these factors, in principle, extend the residence time of the enzyme−substrate hydrogen bond and contribute to their more regiospecific hydroxylation.

It has been postulated that the number of reactive configurations of a substrate in the binding site cavity might be an indication of coupling efficiency.[15,16] Clearly, comparing camphor and norcamphor alone leads to that inference. Tables 8 and 8 show that *d*- and *l*-norcamphor have a smaller fraction of "reactive" configurations than camphor. Camphor is known to have 100% hydroxylation efficiency whereas norcamphor has 12%. However, camphane provides a counter example. It has nearly the same fraction of reactive geometries as camphor (Tables 5 and 6), yet it has a hydroxylation efficiency of 5%. Even if unreactive configurations are redefined to also include those in which the ferryl oxygen is close only to a primary carbon hydrogen atom, as well as those in which it is too far from any H atom to interact with it, the percentage of reactive encounters which are due to hydrogens attached to secondary carbons is comparable for camphane and camphor. Thus, even with this definition, both substrates have comparable fractions of reactive geometries. While the number of reactive encounters is an enticing hypothesis for simulation probes of decoupling, the origin of decoupling is clearly more complex.

Conclusions

Molecular dynamics simulations of four camphor-like substrates of cytochrome $P450_{cam}$ have been characterized. It has been demonstrated that molecular dynamic simulations of the configurations of the enzyme−substrate complex incorporating only the dynamics of residues within 16 Å of the reaction site can be used in conjunction with electronic criteria to make accurate predictions of the regiospecificity of hydroxylation of such substrates. The use of such an approximate model provides information about reaction regiospecificity which is as accurate as full protein simulations for these substrates.

The correctly predicted trends in regiospecificity for camphor, camphane, thiocamphor, and norcamphor based on the mobilities of these substrates in the binding site of $P450_{cam}$ indicate that neither the existence of a hydrogen bond nor the magnitude of van der Waals interactions alone is sufficient to determine the dynamics of such substrates in the active site of $P450_{cam}$. Rather, as suggested by Raag and Poulos,[20] the mobility of such substrates, which determine the regiospecificity of product distribution, is a combination of these factors. Thus, one cannot *a priori* predict such behavior by a cursory examination of substrate composition and architecture. Molecular dynamics studies of the time-dependent enzyme−substrate interactions in conjunction with thermodynamic criteria appear to be a useful tool for making semi/quantitative predictions of reaction profiles using approximate theoretical methods.

Acknowledgment. We gratefully acknowledge support from NIH Grant GM #29743 and an award of C-90 Supercomputer Service Units at the NSF Sponsored Pittsburgh Supercomputing Center.

Supplementary Material Available: AMBER prep file used to establish the assigned atom types and charges from ZINDO Mulliken charges (3 pages). This material is contained in many libraries on microfiche, immediately follows this article in the microfilm version of the journal, can be ordered from the ACS, and can be downloaded from the Internet; see any current masthead page for ordering information and Internet access instructions.

JA933737F